A novel regulatory role of microRNA-5590-3p in hepatocellular carcinoma via the HOXB2/MYC axis

BIN LI[1,2] and LIN ZHOU[1]

[1]Department of Gastroenterology, The First Affiliated Hospital of Zhengzhou University, Zhengzhou, Henan 450052, P.R. China; [2]Department of Nephrology, The Fifth Affiliated Hospital of Zhengzhou University, Zhengzhou, Henan 450052, P.R. China

Received June 3, 2025; Accepted February 12, 2026

DOI: 10.3892/or.2026.9130

Abstract. The present study aimed to investigate the effects of microRNA (miR)-5590-3p on the biological functions of hepatocellular carcinoma (HCC) cells through the homeobox B2 (HOXB2)/MYC axis. The expression levels of miR-5590-3p, HOXB2 and MYC were measured in HCC tissues and cell lines, and the relationships between miR-5590-3p, HOXB2, and the clinicopathological characteristics and prognosis of patients with HCC were analyzed. The Cell Counting Kit-8 assay assessed cell proliferation, flow cytometry measured apoptosis rate, and the Transwell and wound healing assays evaluated the invasive and migratory abilities of cells. The targeting interactions between miR-5590-3p and HOXB2, and between HOXB2 and MYC were assessed. In addition, a subcutaneous HCC xenograft model was established to assess the effects of miR-5590-3p on tumor growth. The results revealed that miR-5590-3p expression was downregulated in HCC tissues and cells, whereas HOXB2 and MYC expression were upregulated. Notably, low miR-5590-3p expression and high HOXB2 expression were both associated with a poor prognosis in patients with HCC. miR-5590-3p directly targeted and suppressed HOXB2, whereas HOXB2 promoted MYC transcription. Furthermore, downregulation of miR-5590-3p enhanced the invasion, migration and proliferation of Huh7 cells, and reduced their apoptotic rate. By contrast, miR-5590-3p overexpression or HOXB2 silencing decreased invasion, migration and proliferation, while increasing apoptosis. Moreover, HOXB2 overexpression reversed the inhibitory effect of miR-5590-3p upregulation on HCC cell proliferation. HOXB2 appeared to promote Huh7 cell proliferation and motility through MYC transcriptional activation, whereas miR-5590-3p overexpression suppressed tumor growth *in vivo*. In conclusion, miR-5590-3p may inhibit HCC cell proliferation and motility, and induce apoptosis by targeting HOXB2 and suppressing MYC transcription.

Correspondence to: Dr Lin Zhou, Department of Gastroenterology, The First Affiliated Hospital of Zhengzhou University, 1 Jianshe East Road, Zhengzhou, Henan 450052, P.R. China
E-mail: zhoulin6762@163.com

Key words: hepatocellular carcinoma, microRNA-5590-3p, homeobox B2, MYC, proliferation, apoptosis, invasion, migration

Introduction

Hepatocellular carcinoma (HCC) is one of the most common malignant tumors, primarily occurring in patients with chronic liver disease and liver cirrhosis (1). In 2024, an estimated 865,000 new cases of primary liver cancer were diagnosed worldwide, with HCC accounting for 80-85% of all cases, making it the sixth most common cancer and the third leading cause of cancer-related mortality (2). HCC can often be diagnosed noninvasively using cross-sectional imaging based on its characteristic multiphase contrast enhancement, rather than relying strictly on tissue biopsy (3). Despite advancements in treatment, including surgery, chemotherapy, radiotherapy and immunotherapy, the prognosis for patients with HCC remains poor, with a high rate of postoperative recurrence and metastasis. Moreover, <50% of patients with HCC survive for 5 years (4). Chronic infection with hepatitis B virus (HBV) or hepatitis C virus (HCV), metabolic syndrome conditions such as obesity and diabetes, and alcohol consumption can induce liver injury. These factors promote hepatic regeneration and progressive damage, ultimately leading to inflammation, fibrosis and carcinogenesis (5). Aberrant DNA methylation is considered a major mediator of molecular alterations in HCC and may serve as a promising biomarker for early cancer diagnosis (6). Therefore, it is essential to explore the molecular mechanisms underlying HCC malignancy and to identify potential biomarkers for effective therapeutic strategies.

The potential microRNA (miRNA/miR)-mRNA network has been implicated in the pathogenesis of HBV-related HCC (7), and miRNA expression profiles may serve as prognostic or diagnostic biomarkers for HCC (8,9). miR-5590-3p has generally been considered to suppress tumor progression in several malignancies, including gastric cancer (10), prostate cancer (11) and triple-negative breast cancer (12). Furthermore, it has been reported that miR-5590-3p acts as an inhibitor of tumor growth and metastasis in HCC (13). The homeobox (HOX) gene family encodes homologous domain-containing proteins that function as transcription factors and possess unique folding structures enabling DNA binding (14,15). According to Huan *et al* (16), HOXB7 promotes HCC malignancy by enhancing stemness and epithelial-mesenchymal

transition. Regarding HOXB2, bioinformatics analyses in the present study predicted it as a potential target of miR-5590-3p. Based on this prediction, the current study further explored the possible miRNA-mRNA regulatory interaction between miR-5590-3p and HOXB2. HOXB2 has been identified as a tumor promoter in several types of cancer, including bladder cancer (17), colorectal cancer (18) and Wilms tumor (19). However, the regulatory mechanism of HOXB2 remains insufficiently investigated. HOX gene activity may also be associated with the Wnt signaling pathway, as HOXB5, HOXB6, HOXB8 and HOXB9 are coexpressed with several canonical Wnt signaling molecules, including MYC (20). Notably, the oncogenic function of MYC has been well established in HCC progression (21). Therefore, the present study aimed to investigate the effects of the miR-5590-3p/HOXB2/MYC axis on HCC, hypothesizing that miR-5590-3p may inhibit HCC development by modulating HOXB2 and MYC expression.

Materials and methods

Ethics statement. The clinical study was approved by the Ethics Committee of The First Affiliated Hospital of Zhengzhou University (Zhengzhou, China; approval no. 2017055). Due to the retrospective nature of the study and the use of anonymized patient data, the requirement for written informed consent was waived by the ethics committee. All animal experiments were approved by the Institutional Animal Care and Use Committee of The First Affiliated Hospital of Zhengzhou University (approval no. 2019053), and were carried out in strict accordance with guidelines related to animal welfare.

Study subjects. The present retrospective cohort study included a total of 72 patients with HCC who underwent radical hepatectomy in the hepatobiliary surgery department of The First Affiliated Hospital of Zhengzhou University between January 2018 and May 2019. Among them, there were 37 male patients and 35 female patients, and the median age of the patients was 62 years (age range, 28-82 years). The specific demographic and clinical baseline characteristics are shown in Table I. The inclusion criteria were as follows: i) No prior treatment before surgery, such as transcatheter hepatic arterial chemoembolization, radiofrequency ablation or immunotherapy; ii) complete virological testing data, including HBV infection status; iii) exclusion of patients with HCV infection; iv) postoperative pathological confirmation of primary HCC; iv) no residual cancer at the surgical margin; and vi) complete clinical data available. HCC and adjacent normal tissues (≥2 cm from the tumor margin and histologically confirmed to be free of residual cancer cells) were preserved in liquid nitrogen. Routine and regular postoperative follow-up was conducted via telephone interviews and outpatient visits. Overall survival was calculated from the time of diagnosis, and follow-up continued for 5 years, ending on June 1, 2024.

Cell culture. The human normal liver cell line MIHA, and the human liver cancer cell lines Huh7, HCCLM3, MHCC97H and Hep3B were cultured in Dulbecco's Modified Eagle Medium (DMEM) supplemented with 10% fetal bovine serum (FBS). All cell lines were obtained from The Cell Bank of Type Culture Collection of the Chinese Academy of Sciences. DMEM and FBS were purchased from Gibco; Thermo Fisher Scientific, Inc. All human-derived cell lines were subjected to short tandem repeat identification before the start of the experiment to verify the cell line identity and exclude cross-contamination. The relevant results are shown in Table SI. Cells were plated in culture dishes and maintained in a humidified incubator at 37˚C with 5% CO_2. When cells reached 80-90% confluence, they were trypsinized, subcultured and those in the logarithmic growth phase were used for subsequent experiments.

Reverse transcription-quantitative PCR (RT-qPCR). Total RNA was extracted from tissues, as well as the human normal liver cell line MIHA, and the human liver cancer cell lines Huh7, HCCLM3, MHCC97H and Hep3B using TRIzol® reagent (cat. no. 15596026; Invitrogen; Thermo Fisher Scientific, Inc.). The concentration and purity of the extracted RNA were determined using a NanoDrop 2000 spectrophotometer (NanoDrop; Thermo Fisher Scientific, Inc.). Subsequently, cDNA was synthesized from total RNA according to the manufacturers' instructions of the TaqMan MicroRNA Assays Reverse Transcription Primer (cat. no. 4427975; Thermo Fisher Scientific, Inc.) and the PrimeScript RT Reagent Kit (cat. no. RR047A; Takara Bio, Inc.). Primers specific to the target genes were designed and synthesized by Takara Bio, Inc. (Table II). qPCR was performed using TaqMan Universal PCR Master Mix (Applied Biosystems; Thermo Fisher Scientific, Inc.) on a 7500 Fast Real-Time PCR System (Applied Biosystems; Thermo Fisher Scientific, Inc.). The qPCR reaction system was prepared according to the kit instructions and the qPCR amplification conditions were as follows: 95˚C for 10 min for initial denaturation; followed by 40 cycles at 95˚C for 10 sec, 60˚C for 20 sec and 72˚C for 34 sec. miR-5590-3p expression levels were normalized to U6, whereas the mRNA expression levels of the other genes were normalized to β-actin. The relative expression levels of target genes were calculated using the $2^{-\Delta\Delta Cq}$ method (22).

Cell grouping and transfection. Huh7 and Hep3B cells were seeded in 6-well plates at a density of $5x10^5$ cells/well and cultured in a 37˚C, 5% CO_2 incubator until they reached ~70% confluence for transfection. Transfection was performed using Lipofectamine® 2000 reagent (cat. no. 11668019; Invitrogen; Thermo Fisher Scientific, Inc.) according to the manufacturer's instructions. The final concentration of miR-5590-3p mimic, mimic-negative control (NC), miR-5590-3p inhibitor, inhibitor-NC, small interfering RNA (siRNA)-NC and siRNA-HOXB2 was 50 nM each; whereas the concentration of HOXB2 overexpression plasmid (Oe-HOXB2) and Oe-NC was 2 μg/well. Oe-HOXB2 and Oe-NC were constructed based on the pcDNA3.1(+) vector backbone (Invitrogen; Thermo Fisher Scientific, Inc.), with Oe-NC serving as an empty vector control without HOXB2 insertion. Various nucleic acids and Lipofectamine 2000 were diluted separately with serum-free medium, mixed after standing at room temperature for 5 min, and incubated at room temperature for 20 min to form transfection complexes, which were then added to the cells for transient transfection. After 6 h of transfection at 37˚C and 5% CO_2, the medium was replaced with complete DMEM containing 10% FBS, and the cells were cultured for a further

Table I. Relationship between the expression of miR-5590-3p and HOXB2 and the clinicopathological parameters of patients with hepatocellular carcinoma.

	miR-5590-3p			HOXB2		
Clinical parameter	High (n=36)	Low (n=36)	P-value	High (n=36)	Low (n=36)	P-value
Sex			0.6376			0.6473
sMale	17	20		18	20	
Female	19	16		18	16	
Age, years			0.4791			0.6115
<60	15	19		16	18	
≥60	21	17		20	18	
Cirrhosis			0.3412			0.3412
Positive	23	18		22	18	
Negative	13	18		14	18	
Child-Pugh grade			0.4621			0.4621
A	25	21		23	21	
B	11	15		13	15	
AFP, μg/l			0.2196			0.0918
<20	26	20		18	24	
≥20	10	16		18	12	
HBV infection			0.1528			0.1982
Yes	12	19		20	16	
No	24	17		16	20	
TNM stage						0.0021
I + II	24	10	0.0019	12	26	
III + IV	12	26		24	10	
Pathological grade			0.0174			0.0147
I + II	25	14		14	24	
III	11	22		22	12	
Tumor embolism			0.2377			0.1184
Yes	22	16		22	16	
No	14	20		14	20	
Recurrence			0.1567			0.064
Yes	15	22		24	18	
No	21	14		12	18	

The comparison of categorical variables was conducted using the χ^2 test. AFP, α-fetoprotein; HBV, hepatitis B virus; TNM, tumor-node-metastasis.

48 h before subsequent experiments. The following groups were established: Inhibitor NC, mimic-NC, miR-5590-3p inhibitor, miR-5590-3p mimic, siRNA-HOXB2, siRNA-NC, miR-5590-3p mimic + Oe-NC and miR-5590-3p mimic + Oe-HOXB2. A total of 48 h post-transfection, the medium was replaced with fresh DMEM containing 10% FBS for subsequent experiments. siRNA-NC, siRNA-HOXB2, Oe-NC and Oe-HOXB2 were obtained from Suzhou GenePharma Co., Ltd. miR-5590-3p mimic, mimic-NC, inhibitor-NC and miR-5590-3p inhibitor were obtained from Guangzhou RiboBio Co., Ltd. The sequences were as follows: miR-5590-3p mimic, sense: 5'-AAUAAAGUUCAUGUAUGGCAA-3', antisense: 5'-UUGCCAUACAUGAACUUUAUU-3'; miR-5590-3p inhibitor, 5'-UUGCCAUACAUGAACUUUA-3'; mimic-NC, sense 5'-UUCUCCGAACGUGUCACGUTT-3', antisense 5'-ACGUGACACGUUCGGAGAATT-3'; inhibitor-NC, 5'-CAGUACUUUUGUGUAGUACAA-3'; si-HOXB2-1, sense 5'-AUCAGCAAUAUACAAUUAUAAAG-3', antisense 5'-CUUUAUAAUUGUAUAUUGCUGAU-3'; si-HOXB2-2, sense 5'-CACCAUUGAAAGCCAUGAAUUUU-3', antisense 5'-AAAAUUCAUGGCUUUCAAUGGUG-3'; siRNA-NC, sense 5'-UUCUCCGAACGUGUCACGU-3', antisense 5'-ACGUGACACGUUCGGAGAA-3'. In the pre-experiment, the siRNA with the best interference effect (si-HOXB2-1) was selected for the subsequent experiments.

Cell Counting Kit (CCK)-8 assay. Huh7 and Hep3B cells in the logarithmic growth phase were detached using 0.25% trypsin

Table II. Quantitative PCR primer sequences.

Gene	PCR primer sequence, 5'-3'
miR-5590-3p	F: GGGCGCAATAAAGTTCATGTATGG
	R: GTGCAGGGTCCGAGGT
	(universal primer)
HOXB2	F: CGCCAGGATTCACCTTTCCTT
	R: CCCTGTAGGCTAGGGGAGAG
MYC	F: GGCTCCTGGCAAAAGGTCA
	R: CTGCGTAGTTGTGCTGATGT
PCNA	F: CCTGCTGGGATATTAGCTCCA
	R: CAGCGGTAGGTGTCGAAGC
MMP2	F: TACAGGATCATTGGCTACACACC
	R: GGTCACATCGCTCCAGACT
MMP9	F: TGTACCGCTATGGTTACACTCG
	R: GGCAGGGACAGTTGCTTCT
Bcl-2	F: GGTGGGGTCATGTGTGTGG
	R: CGGTTCAGGTACTCAGTCATCC
β-actin	F: ATTGCCGACAGGATGCAGA
	R: GAGTACTTGCGCTCAGGAGGA
U6	F: CTCGCTTCGGCAGCACA
	R: GTGCAGGGTCCGAGGT

F, forward; R, reverse; miR-5590-3p, microRNA-5590-3p; HOXB2, homeobox B2.

to prepare a single-cell suspension. After cell counting, 3,000 cells/100 μl were seeded into each well of a 96-well plate and cultured in a 37˚C, 5% CO_2 incubator. A total of 24, 48 and 72 h after transfection, 10 μl CCK-8 reagent (MilliporeSigma) was added to each well, followed by incubation at 37˚C for 2 h. The optical density at 450 nm was measured using a microplate reader (Shanghai Woyuan Technology Co., Ltd.).

Flow cytometry. Huh7 and Hep3B cell apoptosis was analyzed using Annexin V-FITC/propidium iodide (PI) apoptosis detection kit (BD Biosciences). Cells from each group were centrifuged at 300 x g for 5 min at 4˚C, washed with PBS and centrifuged again. After discarding the supernatant, the cells were resuspended in 250 μl binding buffer at a concentration of $1x10^6$ cells/ml. Subsequently, 100 μl cell suspension was transferred to a 5 ml flow tube and incubated with 5 μl Annexin V-APC and 5 μl PI for 5 min in the dark. The mixture was gently mixed and incubated at room temperature (~25˚C) in the dark for 15 min. After adding 400 μl PBS, the samples were analyzed using a flow cytometer (BD FACSCalibur; BD Biosciences), and data were analyzed using FlowJo software (version 10.8.1; FlowJo; BD Biosciences) to calculate the proportion of apoptotic cells. The total apoptosis rate was calculated as the sum of the apoptosis rates observed in the lower right quadrant (early apoptotic cells) and the upper right quadrant (late apoptotic/necrotic cells).

Scratch assay. Huh7 and Hep3B cells were seeded in 6-well plates at a density of $5x10^5$ cells/well and cultured in a 37˚C, 5% CO_2 incubator until they reached 90-100% confluence for the wound healing assay. Subsequently, a sterile ruler was placed to guide the generation of a vertical scratch with a 200-μl pipette tip. Three independent replicate wells were set up for each group. After scratching, the supernatant was carefully aspirated, and the wells were rinsed three times with PBS. The cells were then cultured in a low-serum medium containing 0.5% FBS to minimize the influence of cell proliferation. Images were captured under an inverted optical microscope (Olympus IX71; Olympus Corporation) at 0 and 24 h after scratching. Cell migration rates were quantified using ImageJ software (version 1.53; National Institutes of Health).

Transwell assay. Transwell chambers (pore size, 8 μm; 24-well format; Corning Life Sciences) were used to detect cell invasion. Matrigel (Corning Life Sciences) was removed from a -20˚C freezer and thawed on ice. After thawing, Matrigel and DMEM were mixed at a ratio of 1:8, and 40 μl of the mixture was added to the upper chamber. The chamber was incubated at 37˚C for 4 h to allow the gel to solidify. Subsequently, cells were detached and resuspended in serum-free medium at a density of $3x10^5$ cells/ml; a 150-μl aliquot of the cell suspension was added to the upper chamber and 600 μl DMEM containing 10% FBS was added to the lower chamber. Each experimental group was prepared in triplicate. The Transwell chambers were incubated at 37˚C for 24 h. After culture, non-migrated cells and residual Matrigel on the upper surface of the chamber were gently wiped away with a cotton swab and washed with PBS. Cells were then fixed with 4% paraformaldehyde at room temperature for 30 min and stained with 0.1% crystal violet at room temperature for 30 min. After staining, excess dye was removed by washing with PBS. Images of the stained cells were captured under an inverted optical microscope (Olympus IX71) and the number of invading cells was counted.

Western blotting. Total protein was extracted from tissues and cells using Radio Immunoprecipitation Assay Lysis buffer (cat. no. P0013B; Beyotime Biotechnology). The protein concentration was measured using a BCA protein assay kit (cat. no. P0012; Beyotime Biotechnology). Equal amounts of protein (30 μg) were electrophoresed by SDS-PAGE on 10% gels and transferred to PVDF membranes. The membranes were then blocked with 5% BSA (Sigma-Aldrich; Merck KGaA) at room temperature for 2 h. Subsequently, the membranes were incubated with the following primary antibodies: MYC (cat. no. 18583; 1:1,000; Cell Signaling Technology, Inc.), PCNA (cat. no. 13110; 1:1,000; Cell Signaling Technology, Inc.), MMP2 (cat. no. 40994; 1:1,000; Cell Signaling Technology, Inc.), MMP9 (cat. no. 13667; 1:1,000; Cell Signaling Technology, Inc.), Bcl2 (cat. no. 3498; 1:1,000; Cell Signaling Technology, Inc.), HOXB2 (cat. no. ab220390; 1:1,000; Abcam) and GAPDH (cat. no. 2118; 1:1,000; Cell Signaling Technology, Inc.), overnight at 4˚C. After three washes in PBS-0.1% Tween 20, the membranes were incubated with goat anti-rabbit secondary antibodies (cat. no. 7074; 1:5,000; Cell Signaling Technology, Inc.) at 37˚C for 2 h. ECL solution (cat. no. P0018AM; Beyotime Biotechnology) was then prepared, and the bands were scanned and images were captured in a dark room. ImageJ software was used to semi-quantify the results. GAPDH was used as the internal control.

RNA immunoprecipitation (RIP) assay. The interaction between miR-5590-3p and HOXB2 was examined using an RIP Kit (cat. no. 17-700; MilliporeSigma). Cells were washed twice with pre-chilled PBS and the supernatant was discarded. RIP Lysis Buffer supplied with the kit (supplemented with protease and RNase inhibitors) was added to lyse the cells on ice for 5-10 min. The lysate was then centrifuged at 12,000 x g for 10 min at 4˚C and the supernatant was collected as the RIP input sample (Input); 10% of the supernatant was reserved as the Input control and the remaining portion was used for immunoprecipitation. Subsequently, 50 μl Protein A/G magnetic beads were washed with RIP Wash Buffer and resuspended in 100 μl RIP Wash Buffer. Subsequently, 5 μg rabbit anti-Ago2 antibody (cat. no. NBP2-67121; Novus Biologicals; Bio-Techne) or normal rabbit IgG (cat. no. 12-370; MilliporeSigma) as a NC were added and incubated at room temperature for 30 min to form bead-antibody complexes. Then, 100 μl cell lysate was added to the bead-antibody complexes, and RIP Wash Buffer was added to bring the reaction system to 1 ml. The mixture was incubated at 4˚C overnight with rotation. The bead-protein complex was then collected, digested with proteinase K, and the RNA was extracted for the detection of HOXB2 and miR-5590-3p enrichment levels by RT-qPCR as aforementioned.

Dual-luciferase assay. Potential target genes of miR-5590-3p were predicted using the TargetScan database (https://www.targetscan.org), and potential binding sites in the HOXB2 3'-UTR region were analyzed. Potential binding sites of HOXB2 in the MYC promoter region were predicted using the JASPAR database (https://jaspar.elixir.no/). Dual-luciferase reporter plasmids containing the wild-type (WT) or mutant (MUT) sequence of the HOXB2 3'-UTR (psiCHECK-2 vector; Promega Corporation) and dual-luciferase reporter plasmids containing the WT or binding site MUT sequence of the MYC promoter (pGL3-basic vector; Promega Corporation) were constructed by Shanghai GenePharma Co., Ltd. To evaluate the interaction between miR-5590-3p and HOXB2, Huh7 and Hep3B cells were co-transfected with WT or MUT HOXB2 reporter plasmids and either miR-5590-3p mimic or mimic-NC using Lipofectamine 2000. After 24 h, luciferase activity was measured using a Dual-Luciferase Reporter Assay Kit (cat. no. E1910; Promega Corporation), with *Renilla* luciferase activity serving as the internal control.

Huh7 and Hep3B cells were co-transfected with siRNA-NC or siRNA-HOXB2, and WT or MUT firefly luciferase reporters (MYC-WT or MYC-mut) into Huh7 cells to detect the regulatory effect of HOXB2 on MYC promoter transcriptional activity. Transfection was performed using Lipofectamine 2000 according to the manufacturer's instructions. A total of 48 h after transfection, luciferase activity was detected using the Dual-Luciferase Reporter Assay Kit. Firefly and *Renilla* luciferase activities were sequentially detected using a multifunctional microplate reader (BioTek; Agilent Technologies, Inc.), and the relative activity ratio of *Renilla*/Firefly luciferase was calculated. Each experiment was set up with three independent replicates.

Chromatin immunoprecipitation (ChIP) assay. ChIP assays were performed using a ChIP kit (cat. no. 17-371; MilliporeSigma) to evaluate HOXB2 enrichment at the MYC promoter. Briefly, Huh7 cells at 70-80% confluence were crosslinked with 1% formaldehyde for 10 min at room temperature. Subsequently, 125 mM glycine was added to terminate the cross-linking reaction, and the cells were washed twice with pre-chilled PBS. After cell lysis, chromatin was sonicated to fragments of 200-500 bp using a sonicator (Scientz-IID; Ningbo Xinchi Biotechnology Co., Ltd., China) under conditions of 20 kHz, 4˚C, 10 sec per cycle, with 10 sec intervals, for a total of 15 cycles. The lysate was then centrifuged at 4˚C, 16,000 x g for 10 min, and the supernatant was collected as the chromatin sample. The supernatant was then incubated overnight at 4˚C with an anti-HOXB2 antibody (cat. no. 65130; 1:50; Cell Signaling Technology, Inc.) or control IgG (cat. no. ab172730; 1:100; Abcam). Subsequently, ~40 μl Protein A/G agarose beads (provided in the kit) per reaction system were added and incubated at 4˚C for 2 h to capture the antibody-protein-DNA complexes. After extensive washing, crosslinks were reversed at 65˚C overnight and DNA was then extracted using the standard phenol/chloroform/isoamyl alcohol [25:24:1 (v/v/v)] method (23), and the enrichment of DNA in the MYC promoter region was detected by RT-qPCR as aforementioned.

Subcutaneous xenograft tumor model. A total of 12 6-week-old male BALB/c nude mice (weight,18-22 g) were purchased from Beijing Vital River Laboratory Animal Technology Co., Ltd. (strain code: 401). All animals were housed in an specific pathogen-free-grade animal laboratory under conditions of 22-25˚C temperature, 60-65% relative humidity, and a 12-h light/dark cycle. Animals had free access to standard feed and drinking water. After one week of acclimation, experiments were initiated. All animal experimental procedures were approved by the Animal Ethics Committee of our institution. Huh7 cells in the logarithmic growth phase were resuspended in PBS to prepare a cell suspension of $1x10^7$ cells/ml; subsequently, $1x10^6$ cells in 100 μl PBS were subcutaneously injected were injected into the left flank of each mouse. A tumor volume of ~50 mm^3 was selected as the starting point for intervention to avoid the unstable stage in the early period of transplantation, and to enhance the repeatability and consistency of *in vivo* tumor growth assessment (24,25). The mice were then randomly divided into two groups (n=6/group): i) miR-5590-3p agomir group: Intratumoral injection of 10 nmol miR-5590-3p agomir (Guangzhou RiboBio Co., Ltd.) per mouse, once every 5 days for a total of 3 weeks; ii) agomir-NC group: Intratumoral injection of 10 nmol agomir-NC (Guangzhou RiboBio Co., Ltd.) per mouse, with the same dosing regimen as miR-5590-3p agomir. During the experiment, the long diameter (L) and short diameter (W) of the tumor were measured every 3 days using a vernier caliper, and the tumor volume was calculated according to the formula $V=(L \times W^2)/2$. Humane endpoints set during the experiment included: Tumor volume exceeding 2,000 mm^3, tumor longest diameter exceeding 20 mm, notable weight loss (>20%), markedly decreased activity or the presence of ulcers. In the present study, the tumor volume of all animals did not exceed 2,000 mm^3 (maximum 1,862 mm^3) and the longest diameter did not exceed 20 mm (maximum 19 mm). In the current study, no mice exhibited body weight loss >20%, a marked reduction

in activity or ulceration, thus no animals met the humane endpoint criteria. On day 24 after inoculation, the nude mice were anesthetized. Anesthesia was administered via inhalation of isoflurane (RWD Life Science Co., Ltd.), with an induction concentration of 3-4% and a maintenance concentration of 1.5-2.0%. Medical-grade oxygen (100%) was used as the carrier gas (flow rate: 1.0 l/min), delivered through a small animal anesthesia machine. After the animals completely lost their righting reflex and toe-pinch reflex, they were euthanized by cervical dislocation. Subsequently, the tumor tissues were rapidly and completely dissected to measure their volumes, and the tumor masses were weighed using an electronic balance (Sartorius AG). Portions of the tumor tissues were stored at -80˚C for RT-qPCR and western blot analysis. Each experiment was independently repeated three times.

Statistical analysis. All data were analyzed using SPSS version 22.0 software (IBM Corp.). Measurement data were presented as the mean ± standard deviation. For comparisons between paired samples (such as HCC tissues and corresponding adjacent tissues), a paired Student's t-test was used; for comparisons between two independent samples, an unpaired Student's t-test was employed. Comparisons among multiple groups were analyzed by one-way ANOVA followed by Tukey's post hoc test. CCK-8 assay and tumor volume data in nude mice were analyzed using two-way or mixed ANOVA test followed by Turkey's or Šidák's post-hoc test, as appropriate. For categorical variables, the χ^2 test was predominantly employed. Patients were stratified into high and low expression groups based on the median expression levels of miR-5590-3p and HOXB2. Prognostic survival time was assessed using the Kaplan-Meier method, and differences between curves were compared using the log-rank test. To evaluate the correlation between miR-5590-3p and HOXB2 expression levels in HCC clinical tissue samples, Pearson correlation analysis was performed. $P<0.05$ was considered to indicate a statistically significant difference.

Results

Expression of miR-5590-3p and HOXB2 in tissues and cells, and their association with clinicopathological characteristics. RT-qPCR analysis showed that miR-5590-3p expression was decreased in HCC tissues compared with that in paired adjacent tissues (Fig. 1A). In addition, its expression in Huh7, HCCLM3, MHCC97H and Hep3B cells was lower than that in MIHA cells, with the lowest expression observed in Huh7 cells (Fig. 1B). Conversely, the expression of HOXB2 was elevated in HCC tissues relative to adjacent tissues (Fig. 1C), and its expression in Huh7, HCCLM3, MHCC97H and Hep3B cells was higher than that in MIHA cells, with the highest expression observed in Huh7 cells (Fig. 1D).

A total of 72 paired HCC and adjacent tissues were stratified into high- and low-expression groups based on the median expression levels of miR-5590-3p and HOXB2. No significant associations were observed between their expression and sex, age, cirrhosis, Child-Pugh grade (26), α-fetoprotein level, HBV infection, tumor embolism and recurrence (Table I). However, the expression of miR-5590-3p and HOXB2 in patients with HCC was associated with tumor-node-metastasis (TNM) stage (27) and pathological grade. Patients with advanced TNM stage and poorer pathological grade exhibited lower miR-5590-3p and higher HOXB2 expression, indicating that both markers are closely associated with HCC malignancy. Kaplan-Meier survival analysis further revealed that low miR-5590-3p expression was associated with poor prognosis in HCC (Fig. 1E).

miR-5590-3p suppresses Huh7 cell proliferation and promotes apoptosis. RT-qPCR confirmed that transfection with the miR-5590-3p mimic markedly increased miR-5590-3p expression in Huh7 and Hep3B cells, whereas transfection with the miR-5590-3p inhibitor markedly decreased endogenous miR-5590-3p levels (Fig. 2A), indicating successful establishment of overexpression and inhibition models.

To examine the role of miR-5590-3p in regulating HCC cell proliferation, CCK-8 assays were conducted to quantify changes in cell viability. The results showed that ectopic overexpression of miR-5590-3p markedly suppressed proliferation in both Huh7 and Hep3B cells, whereas inhibition of miR-5590-3p significantly enhanced the proliferative activity of Huh7 and Hep3B cells (Fig. 2B). These findings indicate that miR-5590-3p functions as a negative modulator of HCC cell proliferation.

Cell migratory and invasive behaviors were further evaluated using scratch test and Transwell assays, respectively. miR-5590-3p overexpression led to a pronounced reduction in the number of cells penetrating the Transwell membrane and delayed wound closure in Huh7 and Hep3B cells (Fig. 2C and D). By contrast, silencing miR-5590-3p markedly increased invasive cell counts and accelerated scratch healing. These results suggest that miR-5590-3p restrains HCC cell motility and invasiveness, whereas its suppression promotes acquisition of a more aggressive phenotype.

In addition, flow cytometric analysis demonstrated that miR-5590-3p overexpression significantly increased apoptosis rate in Huh7 cells, while miR-5590-3p inhibition decreased apoptotic rates (Fig. 2E). This indicates that miR-5590-3p facilitates apoptotic progression, whereas its downregulation enables apoptotic resistance.

Taken together, miR-5590-3p overexpression inhibits HCC cell proliferation, migration and invasion while enhancing apoptosis, whereas its suppression produces opposite effects, supporting a tumor-suppressive role of miR-5590-3p in HCC progression.

miR-5590-3p directly targets and negatively regulates HOXB2. To clarify the regulatory relationship between miR-5590-3p and HOXB2, RT-qPCR was first performed to evaluate changes in HOXB2 expression in Huh7 and Hep3B cells following transfection with the miR-5590-3p mimic or inhibitor. Compared with in the NC-transfected cells, suppression of miR-5590-3p notably increased HOXB2 mRNA levels, whereas overexpression of miR-5590-3p markedly reduced HOXB2 expression (Fig. 3A). These expression trends were consistent with the reciprocal patterns observed in clinical HCC tissues, indicating a potential negative regulatory interaction between miR-5590-3p and HOXB2.

Subsequently, bioinformatics prediction using the TargetScan database identified a putative binding site for

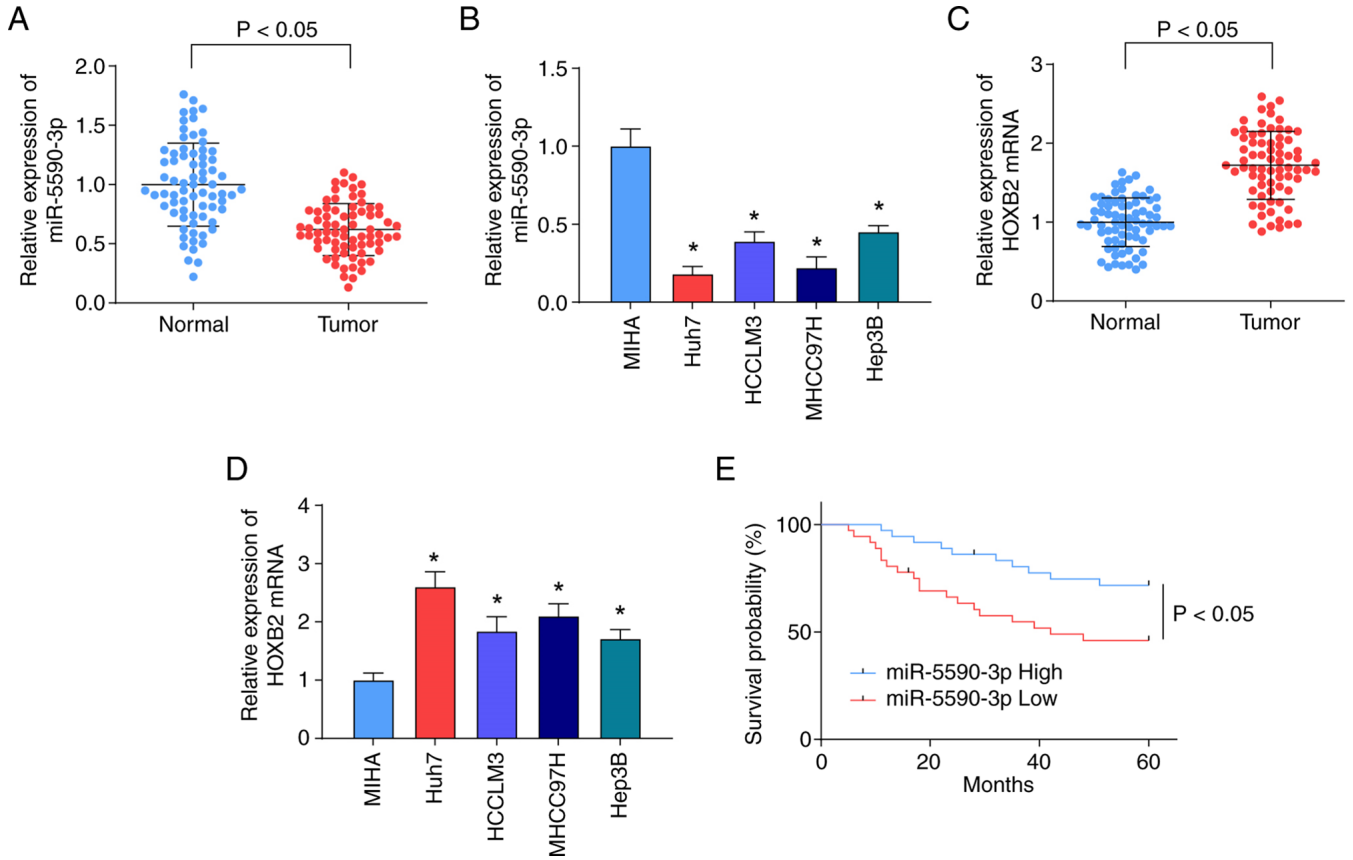

Figure 1. Expression of miR-5590-3p and HOXB2 in tissues and cells. (A) RT-qPCR detection of the expression levels of miR-5590-3p in HCC tissues and adjacent normal tissues (n=72). (B) RT-qPCR detection of the expression levels of miR-5590-3p in various cell lines. (C) RT-qPCR detection of the mRNA expression levels of HOXB2 in HCC tissues and adjacent normal tissues (n=72). (D) RT-qPCR detection of the mRNA expressionl levels of HOXB2 in various cell lines. (E) Effect of miR-5590-3p expression on the overall survival of patients with HCC. *P<0.05 vs. MIHA cells. Data are presented as the mean ± standard deviation. The data were analyzed using (A and C) paired Student's t-test, (B and D) one-way ANOVA followed by Tukey's post hoc test, or (E) Kaplan-Meier analysis with log-rank test. HCC, hepatocellular carcinoma; HOXB2, homeobox B2; miR-5590-3p, microRNA-5590-3p; RT-qPCR, reverse transcription-quantitative PCR.

miR-5590-3p within the 3'-UTR region of HOXB2 that was highly complementary to the miR-5590-3p seed sequence (Fig. 3B). Pearson correlation analysis performed on clinical HCC specimens further demonstrated a significant inverse correlation between miR-5590-3p and HOXB2 expression (Fig. 3C), supporting their antagonistic regulatory relationship *in vivo*.

To validate the direct targeting effect, dual-luciferase reporter constructs containing HOXB2-WT or HOXB2-MUT 3'-UTR sequences were co-transfected into cells with the miR-5590-3p mimic. The luciferase activity of the HOXB2-WT reporter was reduced by miR-5590-3p overexpression, whereas no notable change was observed in the HOXB2-MUT group (Fig. 3D), confirming that miR-5590-3p specifically binds to the 3'-UTR of HOXB2.

Furthermore, RIP assays demonstrated that both miR-5590-3p and HOXB2 mRNA were enriched in Ago2-associated immunoprecipitates (Fig. 3E), indicating that they coexist within the RNA-induced silencing complex and supporting a direct molecular interaction. Survival analysis further revealed that patients with HCC and elevated HOXB2 expression exhibited significantly shorter overall survival (Fig. 3F), suggesting that aberrant HOXB2 upregulation may be closely associated with an unfavorable prognosis.

Collectively, these multi-level experimental findings indicate that HOXB2 is a direct downstream target of miR-5590-3p, and that miR-5590-3p participates in HCC progression by negatively regulating HOXB2 expression.

Silencing HOXB2 suppresses Huh7 cell proliferation. To further elucidate the functional role of HOXB2 in HCC, siRNA-HOXB2 or siRNA-NC was transfected into Huh7 and Hep3B cells. RT-qPCR confirmed that HOXB2 mRNA levels were markedly reduced following siRNA-HOXB2 transfection in both cell lines (Fig. 4A), indicating efficient knockdown. Cell proliferation assays using CCK-8 demonstrated that suppression of HOXB2 decreased the proliferative capacity of Huh7 and Hep3B cells (Fig. 4B). Scratch and Transwell assays further revealed that HOXB2 knockdown markedly delayed scratch closure in Huh7 cells, and significantly reduced invasive activity in both Huh7 and Hep3B cells (Fig. 4C and D), indicating that HOXB2 contributes to HCC cell migration and invasion. In addition, flow cytometric analysis showed that HOXB2 silencing increased the proportion of apoptotic Huh7 cells (Fig. 4E), suggesting that inhibition of HOXB2 facilitates apoptosis in HCC cells.

Taken together, these results demonstrate that HOXB2 promotes proliferation, migration and invasion while inhibiting

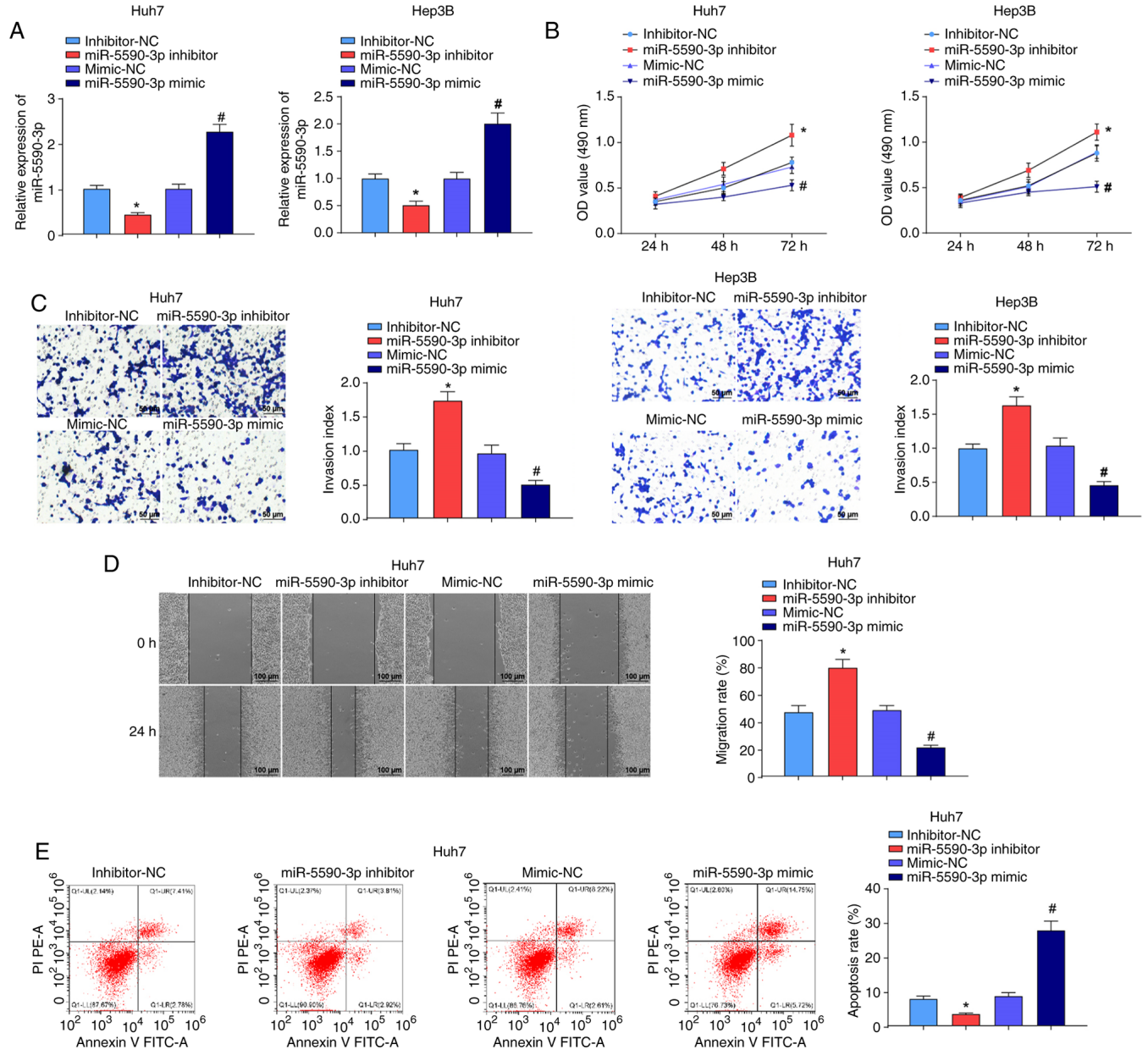

Figure 2. miR-5590-3p suppresses the invasion, migration and proliferation of Huh7 cells while promoting apoptosis. (A) Reverse transcription-quantitative PCR detection of the expression levels of miR-5590-3p in transfected Huh7 and Hep3B cells. (B) Cell Counting Kit-8 assay to detect the proliferation of Huh7 and Hep3B cells. (C) Transwell assay to evaluate invasion of Huh7 and Hep3B cells. (D) Scratch test to assess cell migration. (E) Flow cytometry to detect cell apoptosis. *P<0.05 vs. inhibitor-NC group, #P<0.05 vs. mimic-NC group. Data are presented as the mean ± standard deviation. The data were analyzed using (A and C-E) one-way ANOVA followed by Tukey's post hoc test, or (B) two-way ANOVA followed by Tukey's post hoc test. miR-5590-3p, microRNA-5590-3p; NC, negative control; OD, optical density; PI, propidium iodide.

apoptosis in HCC cells, supporting its tumor-promoting role during HCC progression.

HOXB2 overexpression attenuates the inhibitory effect of miR-5590-3p on Huh7 cell proliferation. To further determine the influence of HOXB2 expression on malignant behaviors of HCC cells, first, RT-qPCR was performed to verify the transfection efficiency of Oe-HOXB2. The results showed that the mRNA expression levels of HOXB2 were significantly increased in the Oe-HOXB2 group compared with those in the Oe-NC group (Fig. 5A). Subsequently, Huh7 and Hep3B cells were co-transfected with the miR-5590-3p mimic and Oe-HOXB2, followed by evaluation of the malignant behaviors of cells in each group, including cell proliferation, migration, invasion and apoptosis. Cell proliferation was detected using the CCK-8 method. The results showed that, compared with in the miR-5590-3p mimic + Oe-NC group, the proliferation of Huh7 and Hep3B cells was significantly increased in the miR-5590-3p mimic + Oe-HOXB2 group (Fig. 5B). Cell invasion was further evaluated using the Transwell assay. The results indicated that, compared with in the miR-5590-3p mimic + Oe-NC group, the membrane-penetrating invasion of Huh7 and Hep3B cells was significantly enhanced in the miR-5590-3p mimic + Oe-HOXB2 group (Fig. 5C). Furthermore, the results of the wound healing assay showed that, compared with in the miR-5590-3p mimic + Oe-NC

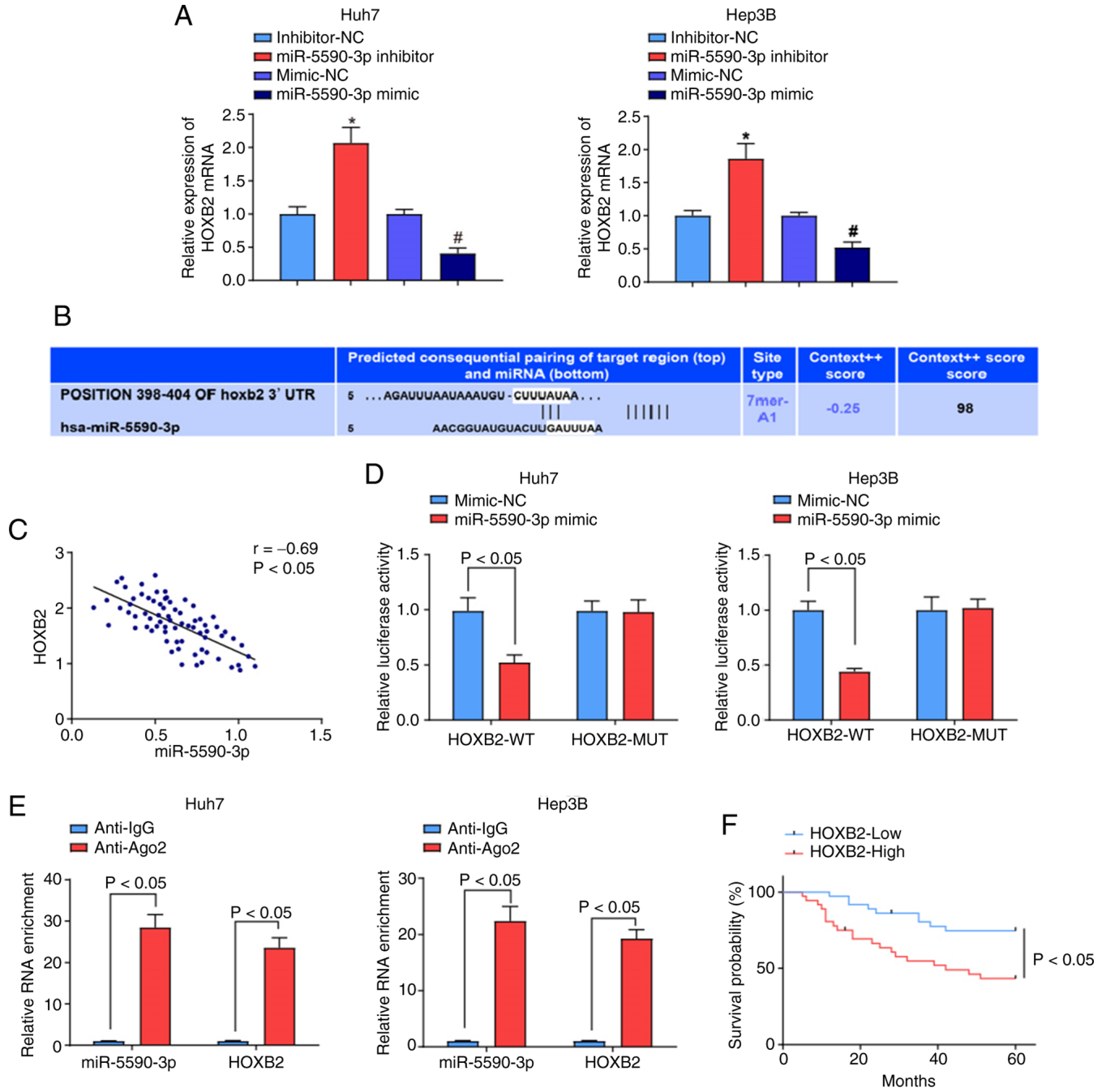

Figure 3. miR-5590-3p targets and negatively regulates HOXB2. (A) Reverse transcription-quantitative PCR detection of HOXB2 mRNA expression in transfected cells. (B) Bioinformatics website prediction of the binding site between miR-5590-3p and HOXB2. (C) Pearson analysis of the correlation between miR-5590-3p and HOXB2 in clinical samples. (D) Dual-luciferase reporter assay to validate the targeting relationship between miR-5590-3p and HOXB2 in Huh7 and Hep3B cells. (E) RNA immunoprecipitation to verify the targeting relationship between HOXB2 and miR-5590-3p in Huh7 and Hep3B cells. (F) Effect of HOXB2 expression on the overall survival of patients with hepatocellular carcinoma. *P<0.05 vs. inhibitor-NC group, #P<0.05 vs. mimic-NC group. Data are presented as the mean ± standard deviation. The data were analyzed using (A) one-way ANOVA followed by Tukey's post hoc test, (C) Pearson correlation test, (D and E) unpaired Student's t-test or (F) Kaplan-Meier analysis with the log-rank test. HOXB2, homeobox B2; miR-5590-3p, microRNA-5590-3p; MUT, mutant; NC, negative control; WT, wild-type.

group, the migration of Huh7 cells was significantly promoted in the miR-5590-3p mimic + Oe-HOXB2 group (Fig. 5D). In addition, flow cytometric analysis of cell apoptosis revealed that, compared with in the miR-5590-3p mimic + Oe-NC group, the proportion of apoptotic Huh7 cells was significantly lower in the miR-5590-3p mimic + Oe-HOXB2 group (Fig. 5E), suggesting that reduced HOXB2 expression may promote apoptosis in HCC cells.

Collectively, these findings indicate that alterations in HOXB2 expression modulate multiple malignant phenotypes of HCC cells, including proliferation, migration, invasion and apoptosis.

HOXB2 promotes Huh7 cell progression through transcriptional activation of MYC. HOXB2 is known to function as a transcriptional regulator and has been implicated in controlling

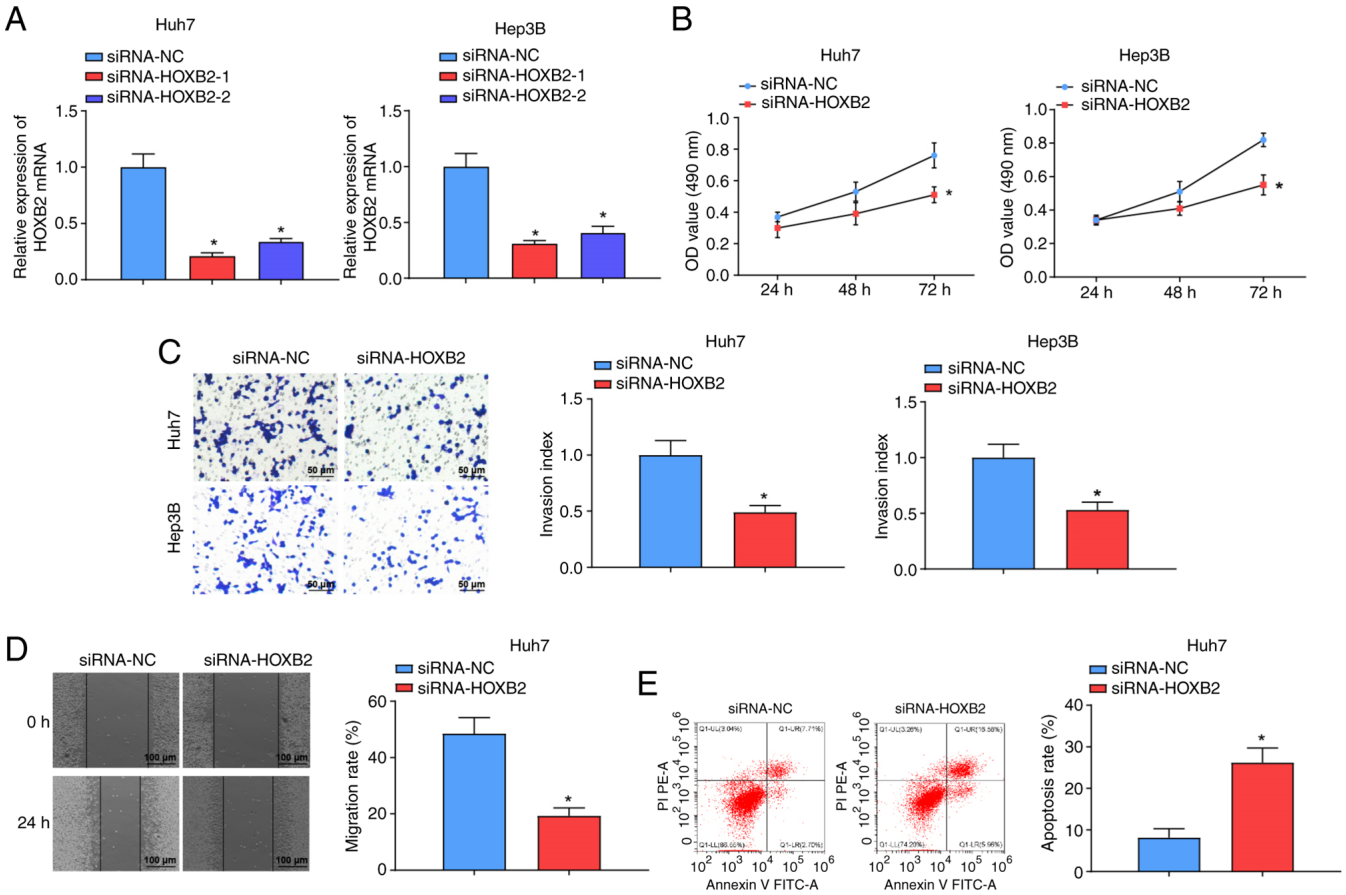

Figure 4. Silencing HOXB2 suppresses invasion, migration and proliferation of Huh7 cells, and facilitates apoptosis. (A) Reverse transcription-quantitative PCR detection of HOXB2 mRNA expression in transfected Huh7 and Hep3B cells. (B) Cell Counting Kit-8 assay to detect proliferation of Huh7 and Hep3B cells. (C) Transwell assay to evaluate invasion of Huh7 and Hep3B cells. (D) Scratch test to assess migration of Huh7 cells. (E) Flow cytometry to detect Huh7 cell apoptosis. *P<0.05 vs. siRNA-NC group. Data are presented as the mean ± standard deviation. The data were analyzed using (A) one-way ANOVA followed by Tukey's post hoc test, (B two-way ANOVA followed by Šidák's post hoc test or (C-E) unpaired Student's t-test. HOXB2, homeobox B2; NC, negative control; OD, optical density; siRNA, small interfering.

downstream gene expression (28). To explore whether HOXB2 mediates HCC cell progression through transcriptional mechanisms, potential HOXB2 binding sites were first predicted using the JASPAR database. A highly conserved binding motif (GCTAATTAAA) was identified within the MYC promoter region (Fig. 6A), suggesting that MYC may be a direct transcriptional target of HOXB2. MYC, as a classic proto-oncogene, serves a crucial role in the occurrence and development of various tumors (29). RT-qPCR analysis showed that MYC expression was significantly elevated in HCC tissues compared with that in adjacent non-tumorous tissues (Fig. 6B). Moreover, MYC mRNA levels were markedly increased in Huh7, HCCLM3, MHCC97H and Hep3B cells relative to normal MIHA cells, with Huh7 cells exhibiting the highest level of expression (Fig. 6C), suggesting aberrant MYC activation in HCC. To verify the regulatory relationship between HOXB2 and MYC, HOXB2 was silenced in Huh7 cells. Downregulation of HOXB2 significantly decreased MYC mRNA expression (Fig. 6D). Dual-luciferase reporter assays further demonstrated that HOXB2 silencing markedly reduced MYC promoter-driven luciferase activity, whereas mutation of the predicted binding site abolished this effect (Fig. 6E), indicating site-specific transcriptional regulation. ChIP assays further confirmed that HOXB2 was directly enriched at the MYC promoter region, and this enrichment was significantly reduced following HOXB2 silencing (Fig. 6F), supporting direct binding of HOXB2 to the MYC promoter at the chromatin level.

To evaluate the functional significance of the HOXB2-MYC axis, Huh7 cells were co-transfected with Oe-HOXB2 and siRNA-MYC. RT-qPCR showed that HOXB2 overexpression increased MYC expression, as well as the levels of proliferation-associated PCNA, migration-associated MMP2 and invasion-associated MMP9, while reducing the expression of the apoptosis-related gene Bcl2; these effects were reversed upon MYC knockdown (Fig. 6G). Western blot analysis yielded consistent results at the protein level (Fig. 6H).

Collectively, these data demonstrate that HOXB2 directly binds to the MYC promoter and activates its transcription, which may regulate gene programs governing proliferation, migration, invasion and apoptosis in HCC cells.

miR-5590-3p overexpression slows xenograft tumor growth in vivo. To further validate the regulatory role of miR-5590-3p in HCC progression at the *in vivo* level, a nude mouse subcutaneous xenograft model was established. Dynamic monitoring of tumor growth demonstrated that, compared with in the control group, xenografts derived from miR-5590-3p-overexpressing cells exhibited markedly attenuated growth (Fig. 7A).

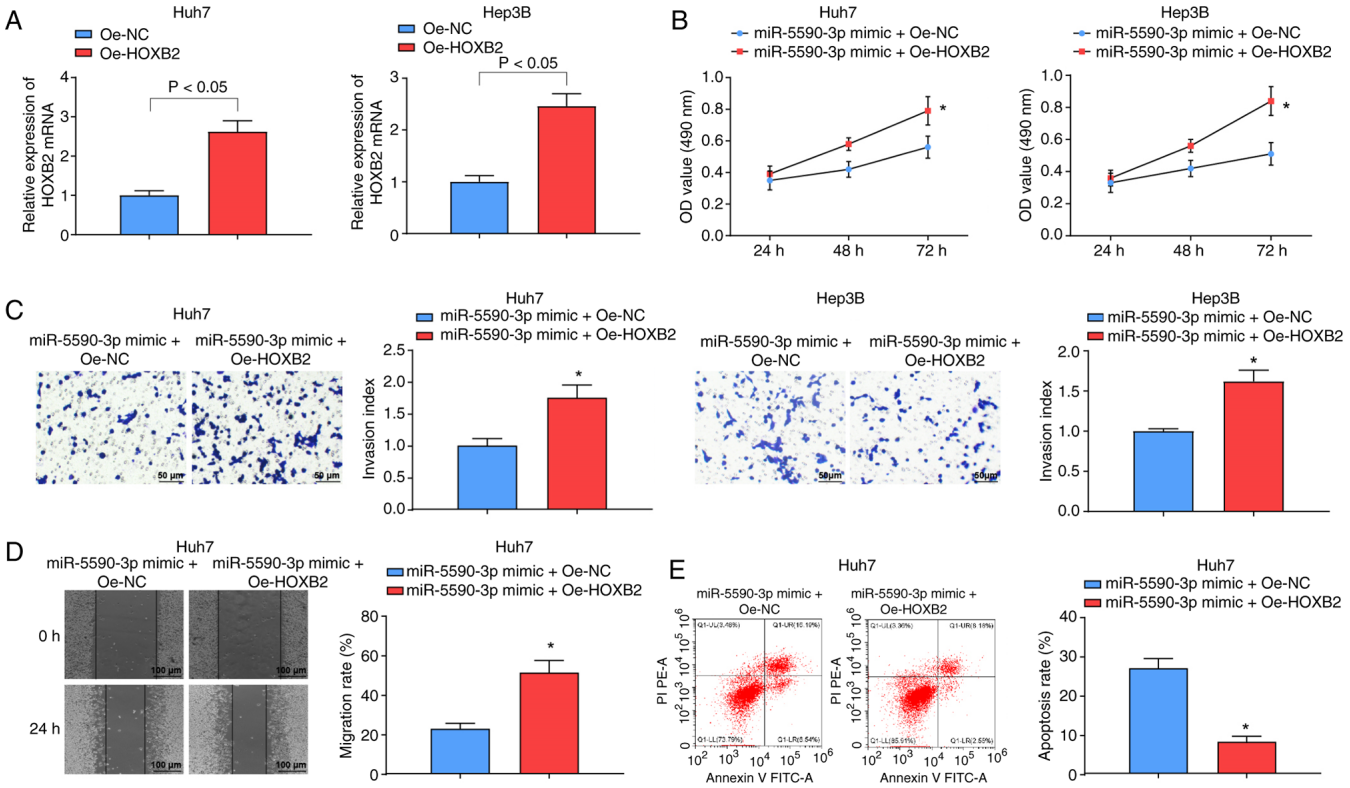

Figure 5. HOXB2 overexpression impairs the inhibitory effect of upregulated miR-5590-3p on Huh7 cells. (A) Reverse transcription-quantitative PCR detection of HOXB2 mRNA expression in transfected Huh7 and Hep3B cells. (B) Cell Counting Kit-8 assay to detect proliferation of Huh7 and Hep3B cells. (C) Transwell assay to evaluate invasion of Huh7 and Hep3B cells. (D) Scratch test to assess migration of Huh7 cells. ∈ Flow cytometry to detect apoptosis of Huh7 cells. *P<0.05 vs. miR-5590-3p mimic + Oe-NC group. Data are presented as the mean ± standard deviation. The data were analyzed using (A and C-E) unpaired Student's t-test or (B) two-way ANOVA followed by Šidák's post hoc test. HOXB2, homeobox B2; miR-5590-3p, microRNA-5590-3p; NC, negative control; OD, optical density; Oe, overexpression plasmid.

Tumor growth curves further showed that the increase in tumor volume was markedly delayed in the miR-5590-3p overexpression group (Fig. 7B). At the experimental endpoint, both tumor volume and tumor weight were significantly reduced compared with those in the control group (Fig. 7C), suggesting that miR-5590-3p effectively inhibits the growth of HCC xenografts *in vivo*.

To further investigate molecular alterations within the miR-5590-3p/HOXB2/MYC axis in xenograft tissues, RT-qPCR and western blot analysis were performed. RT-qPCR results demonstrated that miR-5590-3p expression was increased in xenografts from the overexpression group, whereas the mRNA levels of HOXB2 and MYC were markedly decreased (Fig. 7D). Consistently, western blot analysis confirmed that HOXB2 and MYC protein levels were substantially reduced in tumors overexpressing miR-5590-3p (Fig. 7E).

Collectively, these *in vivo* findings further corroborate that miR-5590-3p overexpression suppresses HCC xenograft growth, and that its tumor-inhibitory effect is accompanied by coordinated downregulation of HOXB2 and MYC, in agreement with the *in vitro* observations.

Discussion

HCC is a common gastrointestinal malignancy characterized by high mortality and poor prognosis (30). The findings of the present study demonstrated that miR-5590-3p inhibits HOXB2 expression through targeted suppression, thereby reducing MYC transcriptional activity and ultimately suppressing HCC cell proliferation, migration and invasion, while promoting apoptosis.

The present study provides evidence that miR-5590-3p expression is downregulated in HCC tissues, and low miR-5590-3p expression in patients with HCC is associated with an advanced TNM stage and higher pathological grade. A previous study also reported that miR-5590-3p is downregulated in HCC, and that long non-coding RNA SOX9 antisense RNA 1-dependent upregulation of miR-5590-3p inhibits the proliferation and metastasis of HCC cells (13). Consistent with the present results, miR-5590-3p expression has been shown to be reduced in renal cell carcinoma, and its upregulation enhances the inhibitory effects of FGD5-AS1 siRNA on cell proliferation and metastasis (31). Moreover, SNHG14-mediated sponging of miR-5590-3p promotes the progression and immune escape of diffuse large B-cell lymphoma by targeting zinc finger E-box-binding HOX 1 (32). In addition, in triple-negative breast cancer, miR-5590-3p expression is decreased in tumor tissues, and restoration of miR-5590-3p expression induces apoptosis, and inhibits the migratory, proliferative and invasive capacities of cancer cells (12). Furthermore, experimental data from a previous study revealed that miR-5590-3p is expressed at low levels in gastric cancer, and its overexpression *in vitro* inhibits cell

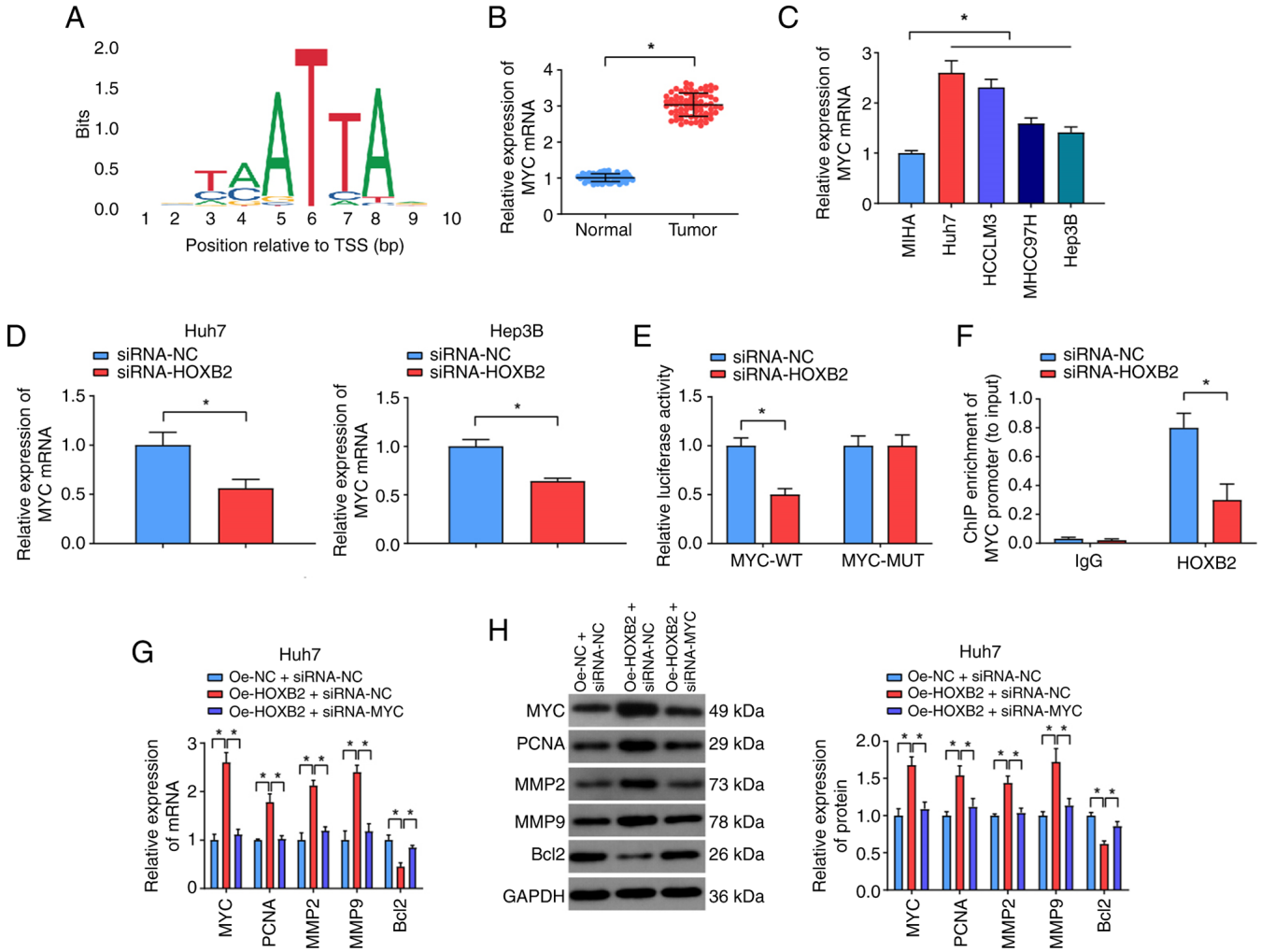

Figure 6. Effects of HOXB2 on Huh7 cell biological behavior via MYC transcriptional regulation. (A) Predicted HOXB2-binding sites within the MYC promoter using the JASPAR database. (B) MYC mRNA expression in hepatocellular carcinoma and adjacent non-tumor tissues detected by RT-qPCR (n=72). (C) MYC mRNA expression in different cell lines. (D) RT-qPCR analysis of MYC mRNA levels following HOXB2 knockdown. (E) Dual-luciferase reporter assay assessing the effect of HOXB2 on MYC promoter activity. (F) Chromatin immunoprecipitation assay detecting HOXB2 enrichment at the MYC promoter region. (G) RT-qPCR analysis of proliferation-, migration-, invasion- and apoptosis-related gene expression following HOXB2 overexpression and/or MYC silencing. (H) Western blot analysis of the expression levels of proteins related to cell biological functions. *P<0.05. All experiments were independently repeated three times. Data are presented as the mean ± standard deviation. The data were analyzed using (B) paired Student's t-test, (C, G and H) one-way ANOVA followed by Tukey's post hoc test or (D-F) unpaired Student's t-test. HOXB2, homeobox B2; NC, negative control; MUT, mutant; Oe, overexpression plasmid; RT-qPCR, reverse transcription-quantitative PCR; siRNA, small interfering; WT, wild-type.

proliferation (10). Taken together, these findings suggest that miR-5590-3p acts as a tumor suppressor in various types of cancer, and targeting miR-5590-3p in malignant cells may represent a promising therapeutic strategy.

The present study subsequently focused on the downstream target of miR-5590-3p, HOXB2, in HCC progression. It was observed that HOXB2 expression was elevated in HCC tissues and cell lines, and functional assays confirmed that HOXB2 silencing suppressed HCC cell proliferation both *in vitro* and *in vivo*. At present, to the best of our knowledge, the functional role of HOXB2 in HCC has not been systematically characterized; however, its oncogenic properties have been documented in other tumor types. For example, HOXB2 is frequently upregulation in glioblastoma, where its elevated expression is associated with poor prognosis and HOXB2 knockdown inhibits the malignant behaviors of cancer cells (33). Moreover, HOXB2 expression is upregulated in cisplatin-resistant non-small cell lung cancer, and miR-139-5p-mediated downregulation of HOXB2 enhances apoptosis and reduces tumor cell proliferation (34). Similarly, it has been shown that HOXB2 expression is increased in esophageal squamous cell carcinoma, and depletion of HOXB2 suppresses tumorigenic progression (35). In addition, findings in ovarian cancer indicate that targeted inhibition of HOXB2 via overexpression of miR-202-5p improves patient survival, and inhibits tumor cell proliferation and metastasis (36). In summary, aberrant upregulation of HOXB2 has been observed in multiple types of cancer and HOXB2 silencing exerts pronounced antitumor effects. To further elucidate the interaction between miR-5590-3p and HOXB2 in HCC cells, additional experiments were performed and it was revealed that HOXB2 overexpression reversed the pro-apoptotic effect induced by miR-5590-3p upregulation, suggesting that miR-5590-3p regulates HCC cell proliferation by modulating HOXB2 expression.

The current study identified a novel regulatory mechanism in which HOXB2 promotes HCC cell proliferation, at

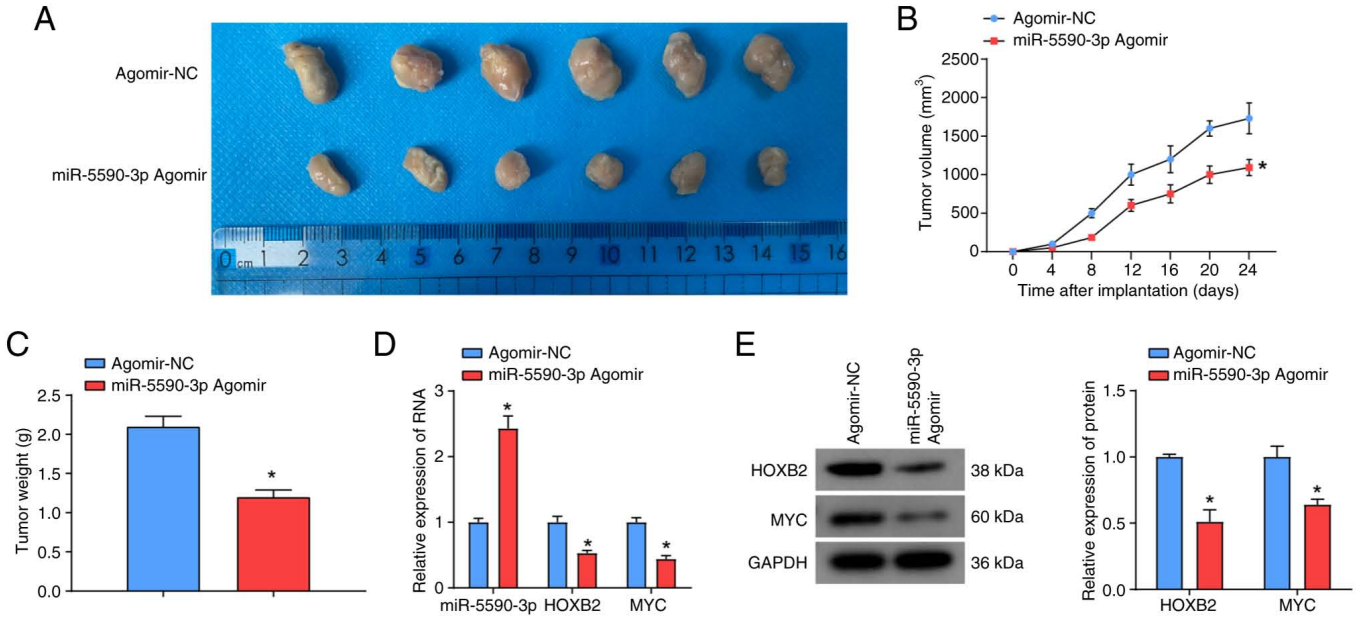

Figure 7. Effects of miR-5590-3p overexpression on HCC xenograft tumor growth. (A) Representative images of subcutaneous HCC xenograft tumors in nude mice. (B) Tumor growth curves. (C) Tumor weight in xenografts. (D) Reverse transcription-quantitative PCR analysis of the expression levels of miR-5590-3p, HOXB2 and MYC. (E) Western blot detection of the protein expression levels of HOXB2 and MYC. *P<0.05 vs. Agomir-NC group. Data are presented as the mean ± standard deviation. Data were analyzed using (B) mixed ANOVA followed by Šidák's post hoc test or (C-E) unpaired Student's t-test. Each group included six mice. HCC, hepatocellular carcinoma; HOXB2, homeobox B2; miR-5590-3p, microRNA-5590-3p; NC, negative control.

least in part through transcriptional activation of MYC. As a member of the HOX gene family, HOXB2 has been implicated in various types of cancer due to its role in regulating cell fate determination and transcriptional programming (37). The present findings revealed that HOXB2 directly binds to the MYC promoter region and enhances its transcription, which aligns with the well-established role of MYC as a key oncogene in HCC (38). It has been shown that HOX family members can participate in cross-talk with oncogenic signaling pathways, such as Wnt and MYC, thereby promoting tumor progression (39). The current study extended these observations by providing direct evidence that HOXB2 transcriptionally activates MYC, leading to increased expression of proliferation (PCNA), migration (MMP2) and invasion (MMP9) markers, while suppressing the expression of the anti-apoptotic gene Bcl2. This regulatory axis may act as a key driver of HCC malignancy. Nevertheless, given the complexity of HCC pathogenesis, additional studies are warranted to determine whether HOXB2 also interacts with other signaling pathways and to validate these findings in clinical specimens.

Although the tumor-suppressive function of miR-5590-3p in HCC has been previously reported, the present study systematically identified HOXB2 as a legitimate downstream target and further revealed a previously unrecognized role of HOXB2 as a transcriptional activator of MYC. These findings delineate a novel 'miRNA-transcription factor-oncogene' regulatory cascade in HCC and provide novel insight into epigenetic-transcriptional interactions underlying hepatocarcinogenesis. From a clinical perspective, the miR-5590-3p/HOXB2/MYC axis exhibits considerable translational relevance. The combined expression pattern characterized by reduced miR-5590-3p and elevated HOXB2 may serve as a potential prognostic biomarker for risk stratification and individualized outcome prediction in patients with HCC. Moreover, this regulatory network offers novel therapeutic opportunities. Restoring miR-5590-3p using a miRNA mimic or pharmacologically targeting HOXB2/MYC signaling may represent promising strategies for patients with aberrant activation of this pathway. Given that MYC remains a challenging direct therapeutic target, modulation of its upstream regulators may provide a more feasible alternative for indirectly attenuating MYC-driven tumor progression.

In conclusion, the present study demonstrated that miR-5590-3p inhibits HCC cell invasion, migration and proliferation, while promoting apoptosis by targeting HOXB2 and suppressing MYC transcription. The discovery of this novel regulatory axis has improved the understanding of the pathogenesis of HCC, and laid a theoretical foundation for the development of prognostic biomarkers and targeted therapeutic strategies based on this axis. Several limitations should be acknowledged. The relatively limited sample size may have reduced statistical power, warranting validation in larger, multi-center cohorts. In addition, *in vivo* rescue experiments were not performed in the present study, and future investigations incorporating appropriate rescue models are needed to further substantiate the causal regulatory relationships within this signaling axis.

Acknowledgements

Not applicable.

Funding

No funding was received.

Availability of data and materials

The data generated in the present study may be requested from the corresponding author.

Authors' contributions

BL designed the study and performed the experiments. LZ performed data analysis and edited the manuscript. BL and LZ confirmed the authenticity of all the raw data. Both authors read and approved the final manuscript.

Ethics approval and consent to participate

The clinical study was approved by the Ethics Committee of The First Affiliated Hospital of Zhengzhou University (approval no. 2017055. Due to the retrospective nature of the study and the use of anonymized patient data, the requirement for written informed consent was waived by the ethics committee. All animal experiments were approved by the Institutional Animal Care and Use Committee of The First Affiliated Hospital of Zhengzhou University (approval no. 2019053), and were carried out in strict accordance with guidelines related to animal welfare.

Patient consent for publication

Not applicable.

Competing interests

The authors declare that they have no competing interests.

References

1. Hu H, Yang L, Li L and Zeng C: Long non-coding RNA KCNQ1OT1 modulates oxaliplatin resistance in hepatocellular carcinoma through miR-7-5p/ABCC1 axis. Biochem Biophys Res Commun 503: 2400-2406, 2018.
2. Lee MH: Public health strategies for hepatocellular carcinoma: From risk factors to prevention and control. J Liver Cancer 25: 204-216, 2025.
3. Huang D, Wei Y, Zhu J and Wang F: Long non-coding RNA SNHG1 functions as a competitive endogenous RNA to regulate PDCD4 expression by sponging miR-195-5p in hepatocellular carcinoma. Gene 714: 143994, 2019.
4. Ding H, Liu J, Zou R, Cheng P and Su Y: Long non-coding RNA TPTEP1 inhibits hepatocellular carcinoma progression by suppressing STAT3 phosphorylation. J Exp Clin Cancer Res 38: 189, 2019.
5. Shimada S, Mogushi K, Akiyama Y, Furuyama T, Watanabe S, Ogura T, Ogawa K, Ono H, Mitsunori Y, Ban D, *et al*: Comprehensive molecular and immunological characterization of hepatocellular carcinoma. EBioMedicine 40: 457-470, 2019.
6. Jiang CG, Chen Q, Wu L, Wang G and Ma J: The innovative regularity and role of p16 methylation in blood during HCC development. J Cancer 9: 1925-1931, 2018.
7. Lou W, Liu J, Ding B, Chen D, Xu L, Ding J, Jiang D, Zhou L, Zheng S and Fan W: Identification of potential miRNA-mRNA regulatory network contributing to pathogenesis of HBV-related HCC. J Transl Med 17: 7, 2019.
8. Wang X, Gao J, Zhou B, Xie J, Zhou G and Chen Y: Identification of prognostic markers for hepatocellular carcinoma based on miRNA expression profiles. Life Sci 232: 116596, 2019.
9. Jiang Y, He J, Li Y, Guo Y and Tao H: The diagnostic value of MicroRNAs as a biomarker for hepatocellular carcinoma: A meta-analysis. Biomed Res Int 2019: 5179048, 2019.
10. Wu N, Han Y, Liu H, Jiang M, Chu Y, Cao J, Lin J, Liu Y, Xu B and Xie X: miR-5590-3p inhibited tumor growth in gastric cancer by targeting DDX5/AKT/m-TOR pathway. Biochem Biophys Res Commun 503: 1491-1497, 2018.
11. Luo ZF, Peng Y, Liu FH, Ma JS, Hu G, Lai SL, Lin H, Chen JJ, Zou GM, Yan Q and Sui WG: Long noncoding RNA SNHG14 promotes malignancy of prostate cancer by regulating with miR-5590-3p/YY1 axis. Eur Rev Med Pharmacol Sci 24: 4697-4709, 2020.
12. Chen FY, Zhou ZY, Zhang KJ, Pang J and Wang SM: Long non-coding RNA MIR100HG promotes the migration, invasion and proliferation of triple-negative breast cancer cells by targeting the miR-5590-3p/OTX1 axis. Cancer Cell Int 20: 508, 2020.
13. Zhang W, Wu Y, Hou B, Wang Y, Deng D, Fu Z and Xu Z: A SOX9-AS1/miR-5590-3p/SOX9 positive feedback loop drives tumor growth and metastasis in hepatocellular carcinoma through the Wnt/β-catenin pathway. Mol Oncol 13: 2194-2210, 2019.
14. No authors listed: Corrigendum for Gao and Chen, volume 315, 2018, p. C675-C686. Am J Physiol Cell Physiol 320: C462, 2021.
15. Liao WT, Jiang D, Yuan J, Cui YM, Shi XW, Chen CM, Bian XW, Deng YJ and Ding YQ: HOXB7 as a prognostic factor and mediator of colorectal cancer progression. Clin Cancer Res 17: 3569-3578, 2011.
16. Huan HB, Yang DP, Wen XD, Chen XJ, Zhang L, Wu LL, Bie P and Xia F: HOXB7 accelerates the malignant progression of hepatocellular carcinoma by promoting stemness and epithelial-mesenchymal transition. J Exp Clin Cancer Res 36: 86, 2017.
17. Liu J, Li S, Cheng X, Du P, Yang Y and Jiang WG: HOXB2 is a putative tumour promotor in human bladder cancer. Anticancer Res 39: 6915-6921, 2019.
18. Li H, Zhu G, Xing Y, Zhu Y and Piao D: miR-4324 functions as a tumor suppressor in colorectal cancer by targeting HOXB2. J Int Med Res 48: 300060519883731, 2020.
19. Jing P, Zou J, Zhang L, Wang C, Yang Y, Deng L and Zhao D: HOXB2 and FOXC1 synergistically drive the progression of Wilms tumor. Exp Mol Pathol 115: 104469, 2020.
20. Wu G, Li X, Liu Y, Li Q, Xu Y and Wang Q: Study on HOXBs of clear cell renal cell carcinoma and detection of new molecular target. J Oncol 2021: 5541423, 2021.
21. Dong R, Wang T, Dong W, Zhang H, Li Y, Tao R, Liu Q, Liang H, Chen X, Zhang B and Zhang X: TGM2-mediated histone serotonylation promotes HCC progression via MYC signalling pathway. J Hepatol 83: 105-118, 2025.
22. Livak KJ and Schmittgen TD: Analysis of relative gene expression data using real-time quantitative PCR and the 2(-Delta Delta C(T)) method. Methods 25: 402-408, 2001.
23. Tammen SA, Dolnikowski GG, Ausman LM, Liu Z, Kim KC, Friso S and Choi SW. Aging alters hepatic DNA hydroxymethylation, as measured by liquid chromatography/mass spectrometry. J Cancer Prev 19: 301-308, 2014.
24. Hoffmann B, Lange T, Labitzky V, Riecken K, Wree A, Schumacher U and Wedemann G: The initial engraftment of tumor cells is critical for the future growth pattern: A mathematical study based on simulations and animal experiments. BMC Cancer 20: 524, 2020.
25. Hather G, Liu R, Bandi S, Mettetal J, Manfredi M, Shyu WC, Donelan J and Chakravarty A: Growth rate analysis and efficient experimental design for tumor xenograft studies. Cancer Inform 13 (Suppl 4): S65-S72, 2014.
26. Pugh RN, Murray-Lyon IM, Dawson JL, Pietroni MC and Williams R: Transection of the oesophagus for bleeding oesophageal varices. Br J Surg 60: 646-649, 1973.
27. Detterbeck FC, Woodard GA, Bader AS, Dacic S, Grant MJ, Park HS and Tanoue LT: The proposed ninth edition TNM classification of lung cancer. Chest 166: 882-895, 2024.
28. Yang X, Tong Y, Ye W and Chen L: HOXB2 increases the proliferation and invasiveness of colon cancer cells through the upregulation of CCT6A. Mol Med Rep 25: 174, 2022.
29. Dhanasekaran R, Deutzmann A, Mahauad-Fernandez WD, Hansen AS, Gouw AM and Felsher DW: The MYC oncogene-the grand orchestrator of cancer growth and immune evasion. Nat Rev Clin Oncol 19: 23-36, 2022.
30. Sun X, Zhuo XB, Hu YP, Zheng X and Zhao QJ: A novel matrine derivative WM622 inhibits hepatocellular carcinoma by inhibiting PI3K/AKT signaling pathways. Mol Cell Biochem 449: 47-54, 2018.

31. Yang Y, Dong MH, Hu HM, Min QH and Xiao L: LncRNA FGD5-AS1/miR-5590-3p axis facilitates the proliferation and metastasis of renal cell carcinoma through ERK/AKT signalling. Eur Rev Med Pharmacol Sci 24: 8756-8766, 2020.
32. Zhao L, Liu Y, Zhang J, Liu Y and Qi Q: LncRNA SNHG14/miR-5590-3p/ZEB1 positive feedback loop promoted diffuse large B cell lymphoma progression and immune evasion through regulating PD-1/PD-L1 checkpoint. Cell Death Dis 10: 731, 2019.
33. Zhou K, Wang W, Zhao W, Li L, Zhang M, Guo P, Zhou C, Li M, An J, Li J and Li X: Benefits of a WeChat-based multimodal nursing program on early rehabilitation in postoperative women with breast cancer: A clinical randomized controlled trial. Int J Nurs Stud 106: 103565, 2020.
34. Du H, Bao Y, Liu C, Zhong A, Niu Y and Tang X: miR-139-5p enhances cisplatin sensitivity in non-small cell lung cancer cells by inhibiting cell proliferation and promoting apoptosis via the targeting of Homeobox protein Hox-B2. Mol Med Rep 23: 104, 2021.
35. Zhang Z, Liang X, Ren L, Zhang S, Li S, Wan T, Xu D and Lv S: LINC00662 promotes cell viability and metastasis in esophageal squamous cell carcinoma by sponging miR-340-5p and upregulating HOXB2. Thorac Cancer 11: 2306-2315, 2020.
36. Yu HY and Pan SS: MiR-202-5p suppressed cell proliferation, migration and invasion in ovarian cancer via regulating HOXB2. Eur Rev Med Pharmacol Sci 24: 2256-2263, 2020.
37. Oh JH, Kim CY, Jeong DS, Kim YC, Kim MH and Cho JY: The homeoprotein HOXB2 limits triple-negative breast carcinogenesis via extracellular matrix remodeling. Int J Biol Sci 20: 1045-1063, 2024.
38. Liu F, Liao Z and Zhang Z: MYC in liver cancer: Mechanisms and targeted therapy opportunities. Oncogene 42: 3303-3318, 2023.
39. Shenoy US, Adiga D, Kabekkodu SP, Hunter KD and Radhakrishnan R: Molecular implications of HOX genes targeting multiple signaling pathways in cancer. Cell Biol Toxicol 38: 1-30, 2022.